ResearchGate

See discussions, stats, and author profiles for this publication at: https://www.researchgate.net/publication/279988399

Metal Iodate–Based Energetic Composites and Their Combustion and Biocidal Performance

ARTICLE *in* ACS APPLIED MATERIALS & INTERFACES · JULY 2015

Impact Factor: 6.72 · DOI: 10.1021/acsami.5b04589 · Source: PubMed

READS

42

6 AUTHORS, INCLUDING:

Haiyang Wang

Nanjing University of Science and Technology

12 PUBLICATIONS **37** CITATIONS

SEE PROFILE

Guoqiang Jian

Applied Materials

44 PUBLICATIONS **719** CITATIONS

SEE PROFILE

Jeffery B DeLisio

University of Maryland, College Park

10 PUBLICATIONS **23** CITATIONS

SEE PROFILE

Available from: Guoqiang Jian
Retrieved on: 31 January 2016

ACS APPLIED MATERIALS & INTERFACES

Research Article

www.acsami.org

Metal Iodate-Based Energetic Composites and Their Combustion and Biocidal Performance

H. Wang,[†] G. Jian,[†] W. Zhou,[†] J. B. DeLisio,[†] V. T. Lee,[‡,§] and M. R. Zachariah*[,†]

[†]Department of Chemical and Biomolecular Engineering and Department of Chemistry and Biochemistry, University of Maryland, College Park, Maryland 20742, United States

[‡]Department of Cell Biology and Molecular Genetics, University of Maryland, College Park 20740, Maryland, United States

Supporting Information

ABSTRACT: The biological agents that can be weaponized, such as *Bacillus anthracis*, pose a considerable potential public threat. Bacterial spores, in particular, are highly stress resistant and cannot be completely neutralized by common bactericides. This paper reports on synthesis of metal iodate-based aluminized electrospray-assembled nanocomposites which neutralize spores through a combined thermal and chemical mechanism. Here metal iodates ($Bi(IO_3)_3$, $Cu(IO_3)_2$, and $Fe(IO_3)_3$) act as a strong oxidizer to nanoaluminum to yield a very exothermic and violent reaction, and simultaneously generate iodine as a long-lived bactericide. These microparticle-assembled nanocomposites when characterized in terms of reaction times and temporal pressure release show significantly improved reactivity. Furthermore, sporicidal performance superior to conventional metal-oxide-based thermites clearly shows the advantages of combining both a thermal and biocidal mechanism in spore neutralization.

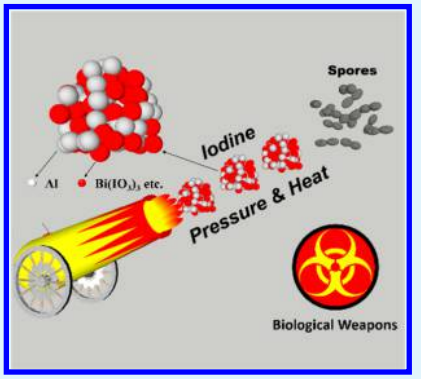

KEYWORDS: *energetic materials, metal iodate, nanothermite, biocidal, electrospray*

1. INTRODUCTION

Thermites is a class of energetic materials that can undergo fast redox reaction between a fuel (e.g., Al) and an oxidizer (CuO, Fe_2O_3, Bi_2O_3, etc.), which ,once initiated, release large amounts of thermal energy.

$$\mathrm{Al} + \frac{3}{2}\mathrm{MO} \rightarrow \frac{1}{2}\mathrm{Al_2O_3} + \frac{3}{2}\mathrm{M} + \Delta H \quad (1)$$

Decreasing the reactant length scales from the micron to the nanoscale greatly increases the interfacial contact and reduces the diffusion distance between fuel and oxidizer, resulting in as much as ~1000× higher reactivity.[1−6] The thermochemical properties of the materials used result in energy densities, for the most common mixtures, that are a factor of 2 or more higher on a volumetric basis than conventional organic-based energetic materials (e.g., TNT or RDX).[7−22]

The potential threats from biological-based weapons, such as those employing *Bacillus anthracis*, pose a significant challenge to global security. Of particular concern are spores of virulent bacteria that are highly stress resistant and cannot be completely killed by high-pressure processing (HPP), heat, or toxic chemicals such as iodophor.[23−25] Conventional energetic materials produce a thermal event over a relatively short time, which may not be sufficient for total inactivation. Thus, a strategy has developed in which, in addition to the thermal event, a remnant biocidal agent delivered simultaneously would have a much longer exposure time resulting in a more effective inactivation. As such, both silver- or halogen-containing thermites, even difluoroiodate compound-based explosives, have been considered as biological agent defeating ingredients.[26−29] The two most common methods of incorporating biocidal agents into energetic systems are to either directly add silver or halogen into the metallized energetic materials or to employ silver- or iodine-containing oxidizers into the thermite formulation.[30−32] The latter option has the potential for Ag and I to act as part of the energy release landscape rather than as a passive species. Some extremely strong oxidizers of the latter kind, such as $NaIO_4/KIO_4$, do not release iodine, while others like I_2O_5 and $AgIO_3$ have storage issues because of their hygroscopicity and light sensitivity.[31,32] The ideal oxidizer should (1) be easy to handle and (2) decompose to allow the oxygen to react with the fuel and release molecular iodine.

$$\mathrm{Al} + \frac{1}{2}\mathrm{M(IO_3)} \rightarrow \frac{1}{2}\mathrm{Al_2O_3} + \frac{1}{2}\mathrm{M} + \frac{1}{4}\mathrm{I_2} + \Delta H \quad (2)$$

In this paper, three metal iodate nanoparticles, $Bi(IO_3)_3$, $Cu(IO_3)_2$, and $Fe(IO_3)_3$, were synthesized and subsequently assembled with aluminum nanoparticles using an electrospray technique to create microsized nanothermites. The confined burning pressure of the metal iodate-based thermite was found to be ~5× higher than conventional Al/CuO nanothermite. The rapid reaction mechanism and the iodine release from the metal-iodate-based thermite was investigated using rapid heating mass spectrometry. The effectiveness of synthesized

Received: May 26, 2015
Accepted: July 10, 2015

ACS Publications © XXXX American Chemical Society

DOI: 10.1021/acsami.5b04589
ACS Appl. Mater. Interfaces XXXX, XXX, XXX−XXX

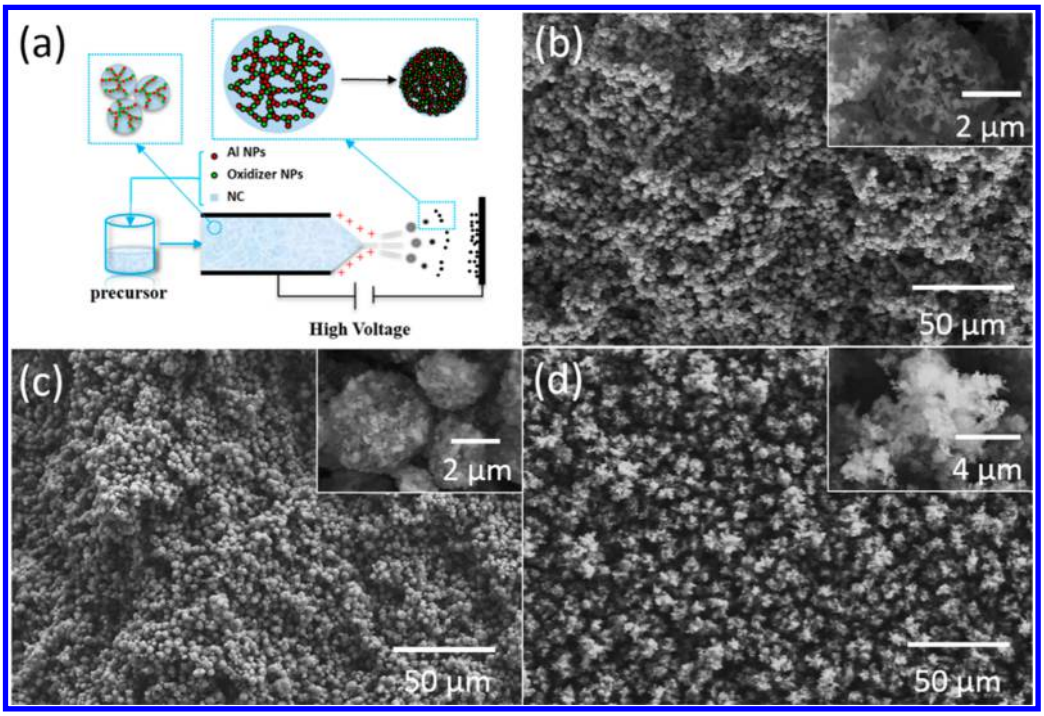

Figure 1. (a) Schematic of electrospray approach. (b–d) Low- and high-magnification SEM images of (b) Al/$Bi(IO_3)_3$ composites, (c) Al/$Cu(IO_3)_2$ composites, and (d) Al/$Fe(IO_3)_3$ composites. Note: all the above composites contain 5% NC (by weight).

iodate-based thermites as a biocidal agent was tested, and results show superior performance in the inactivation of spores.

2. EXPERIMENTAL SECTION

Chemicals. Copper oxide (~50 nm), bismuth oxide (90–210 nm), and iron oxide (~50 nm) were purchased from Sigma-Aldrich, and aluminum (ALEX, ~50 nm) was purchased from Argonide Corp. Al nanoparticles contain ~70% active aluminum (by weight), which is confirmed by thermogravity analysis.[33] Collodion solution (4–8% nitrocellulose, i.e., NC, in ethanol/diethyl ether, by weight) was purchased from Fluka Corp., and diethyl ether (99.8%)/ethanol (99.8%) mixture (volume ratio: 1:3) was employed to dissolve the collodion. The copper iodate, bismuth iodate, and iron iodate nanoparticles were synthesized by the following procedures. The formation energies of these oxidizers were calculated on the basis of the data at https://materialsproject.org/. The formation energies of $Bi(IO_3)_3$, $Cu(IO_3)_2$, and $Fe(IO_3)_3$ are calculated as −1282, −725, and −1293 kJ/mol, respectively.

Synthesis of the Copper Iodate Nanoparticles. Copper iodate nanoparticles were synthesized by milling copper(II) nitrate trihydrate (Sigma-Aldrich) and potassium iodate (Sigma-Aldrich) mixture (mass ratio: 1:3). After the milling process, the sample was washed with 30 mL of deionized water, and centrifuged for 30 min at 13 500 rpm (Hermle Z300). The whole process was repeated 4 times to enable full removal of any impurities. The sample was then dried at 100 °C overnight. The yield of copper iodate nanoparticles using this milling process was ~75%.

Preparation of the Bismuth Iodate and Iron Iodate Nanoparticles. Bismuth iodate ($Bi(IO_3)_3$) and iron iodate ($Fe(IO_3)_3$) nanoparticles were synthesized by a precipitation method. $Bi(IO_3)_3$ nanoparticles were synthesized by the following process: 485 mg bismuth nitrate pentahydrate ($Bi(NO_3)_3{\cdot}5H_2O$) was dissolved in 8 mL nitric acid solution (2 M), and 528 mg iodic acid (HIO_3) was dissolved in 8 mL deionized (DI) water. These were then mixed by dropwise addition of $Bi(NO_3)_3$ solution. The yield of bismuth iodate nanoparticles using this milling process was ~90%. $Fe(IO_3)_3$ nanoparticles were synthesized by mixing the $Fe(NO_3)_3$ solution and HIO_3 solution (1:3, by mole) at concentrations of 25 and 66 mg/mL, respectively. The obtained brown solution was kept at 100 °C overnight, and the subsequent yellow-green precipitate was collected and further washed and dried for characterization, with a yield of ~75%. Both of the $Bi(IO_3)_3$ and $Fe(IO_3)_3$ powders were handled with the same washing, centrifuging, drying, and breaking process as the $Cu(IO_3)_2$.

Preparation of the Physically Mixed Metal Iodate and Metal-Oxide-Based Composites. The traditional approach to create a nanocomposite thermite is by physical mixing. For example, to make the bismuth-iodate-based thermite, 160 mg $Bi(IO_3)_3$ powder was dispersed in 1.8 mL of ethanol and sonicated for 60 min. Then, 51 mg of aluminum nanoparticles (and 0.20 mL collodion for the case of added NC, from Fluka Corp.) is added and sonicated for another 60 min. The suspension was stirred for 24 h, and then allowed to air-dry in a hood. The dry powder was then gently broken to a fine powder. A similar procedure was employed for the other iodates, but the mass was adjusted to maintain a stoichiometry.

Electrospray Procedure. The electrospray assembly process is essentially as previously described in ref 22. For example to make the bismuth-iodate-based thermite 160 mg $Bi(IO_3)_3$ powder was dispersed in 1.8 mL of ethanol and sonicated for 60 min. To this was added 51 mg of aluminum nanoparticles (and 0.20 mL collodion for the case with NC), and the mixture was sonicated for another 60 min. Then, after stirring for 24 h, the suspension was ready to be electrosprayed. The electrospray system consisted of a syringe pump to feed the precursor at a constant speed of 4.5 mL/h, through a stainless steel 0.43 mm inner diameter needle. The distance between the needle and substrate was 10 cm, with an applied voltage of 19 kV.

SEM/EDS, TEM, and TGA/DSC. Scanning electron microscope (SEM) characterization was conducted with a Hitachi SU-70 instrument coupled to an energy dispersive spectrometer (EDX). Transmission electron microscope (TEM) analysis employed a JEOL 2100F field-emission instrument. Thermogravimetry/differential scanning calorimetry (TG/DSC) results were obtained with a TA Instruments Q600 at a rate of 10 °C/min up to a maximum temperature of 1000 °C in a nitrogen atmosphere.

Combustion Cell and Burning Products. The details of combustion cell experiment can be found in refs 5 and 34. A confined combustion cell with a constant volume (~13 cm^3) was used to measure the pressure and burn time of the samples. In this study, 25.0 mg of the loose thermite sample was placed inside a cell and was

DOI: 10.1021/acsami.5b04589
ACS Appl. Mater. Interfaces XXXX, XXX, XXX–XXX

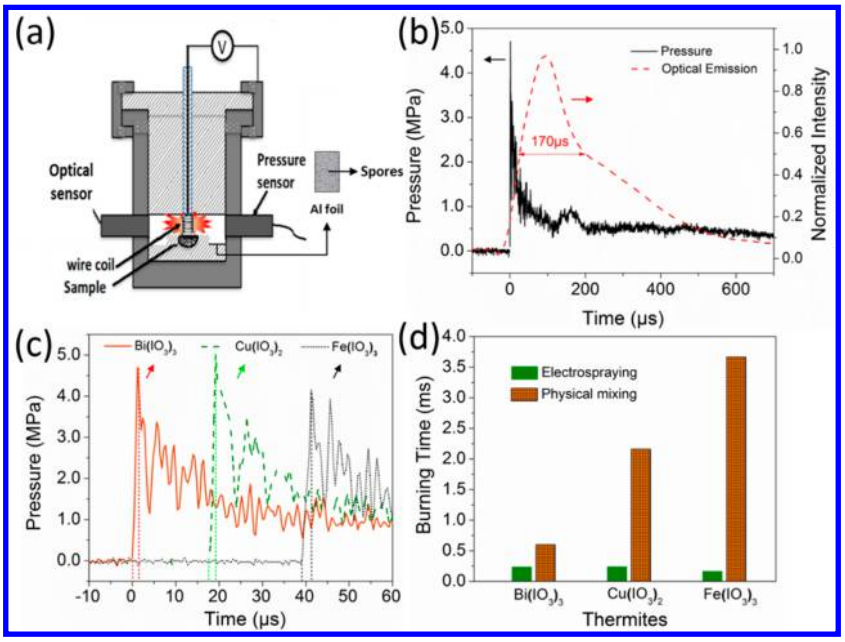

Figure 2. (a) Schematic of combustion cell. (b) Pressure and optical emission profiles of the Al/$Bi(IO_3)_3$ nanothermite composites. (c) Pressure profiles of the three metal-iodate-based thermites. (d) Burning times of metal-iodate-based nanothermite composites. Note: The pressure traces of $Cu(IO_3)_2$- and $Fe(IO_3)_3$-based thermites have been offset to the right, for better readability.

ignited by a nichrome coil on top of the loose powder. An attached piezoelectric pressure sensor (PCB) together with an in-line charge amplifier and signal conditioner were used to record the pressure history. The optical emission history was simultaneously collected by a lens tube assembly, containing a planoconvex lens (f = 50 mm) and a photodetector to collect the broadband emission. The burn time was defined as the peak width at half height of the optical emission.

T-Jump Ignition and Time-Resolved Mass Spectrometry Measurement. The details of the time-of-flight mass spec system used can be found in refs 5 and 33−35. In a typical experiment, a fine Pt wire (76 μm in diameter, 10 mm in length) was coated with a thin layer of sample (3−5 mm in length). An applied voltage of ~24 V was put across the wire to rapidly heat to ~1800 K at a heating rate of 5 × 10^5 K s^{-1}. The wire temperature can be calculated by determining the resistance changing with time. Time-resolved mass spectra were used for characterization of the species produced during the rapid heating. A Vision Research Phantom v12.0 digital camera was employed to capture the burning of the thermite in air. The resolution used was 256 × 256 pixels, and the frame rate used was 67 065 fps (14.9 μs per frame).

Spore Inactivation. The above combustion cell was employed as a container to evaluate the spore inactivation effectiveness of the samples. First, metal-iodate-based thermite was placed in the cell of the internal chamber in the combustion cell (Figure 2a). Aluminum foil was adopted as the substrate for *Bacillus thuringiensis* spores, a known surrogate for *Bacillus anthracis*. A 10 μL portion of spore solution (~7 × 10^5/μL, ~1.4 μg) was dripped onto the foil surface followed by spreading and drying. Aluminum foils deposited with or without spores were placed close to the wall of the chamber, ~15 mm from thermite sample. After ignition, the combustion cell was kept closed for 30 min, following which the foils were extracted and sent for bacterial spore counting assay. Before the test, explosion-product-loaded control foils were deposited with the same amount of spores. Each foil was then immersed in 1 mL of fresh Lysogeny Broth (LB) medium and incubated at 37 °C for 3 h. Our preliminary test reveals that this time period is necessary for the initially immobile living spores to detach from the foil and germinate in the media, enabling us to measure the spore counts quantitatively later. Since the exact range of spore viability was unknown, a serial dilution was used. A 100 μL portion of the medium was extracted and diluted subsequently, with each dilution of a factor of 10. Then 10 μL of these diluted media with different bacteria concentrations were spread in parallel lines on an agar plate. Agar plates were kept overnight at room temperature prior to numeration of the colony forming units (CFUs) in each line. The final counts of spores in each sample were obtained statistically in terms of these serial CFUs. Each experiment was repeated in triplicate.

3. RESULTS AND DISCUSSION

3.1. Metal-Iodate-Based Thermite Synthesis and Assembly. In this work, micron-scale metal-iodate-based energetic composites were produced by electrospraying a precursor solution containing nanoscale components, comprising fuel (nano-Aluminum), the biocidal oxidizer (metal iodates), and a small quantity of energetic binder nitrocellulose. As shown in Figure 1a, because of the combined action of electrostatic forces and surface tension, the precursor suspension shatters into nearly monodiserse microsized droplets. Subsequent rapid evaporation of the solvent drives gelling process within the droplet until the aggregate particles jam, creating a porous structure. More details of the electrospray assembly technique can be found in our prior work.[22,36]

The metal iodate nanoparticles used in this study include bismuth iodate (~90 nm), iron iodate (~70 nm), and copper iodate (~65 nm), which were prepared by either precipitation or milling (see Experimental Section and Supporting Information). For comparison purposes, physically mixed metal-iodate-based nanothermites were also prepared, and the SEM images can be found in Figure S9 in the Supporting Information.

Figure 1b−d shows typical SEM images of the three metal-iodate-based thermites. The obtained Al/$Bi(IO_3)_3$ (Figure 1b) composites have a size distribution of 3−5 μm, have a porous structure, and contain a well-dispersed mixture of the fuel and oxidizer nanoparticles. Al/$Cu(IO_3)_2$ composites have similar structure features and a relatively narrow size of 2−4 μm (Figure 1c), respectively, while the Al/$Fe(IO_3)_3$ composites

DOI: 10.1021/acsami.5b04589
ACS Appl. Mater. Interfaces XXXX, XXX, XXX−XXX

(Figure 1d) were found to have a more open structure, with a larger size ranging from 5 to 7 μm.

3.2. Reactivity of Metal-Iodate-Based Nanothermite. The reactivity of nanothermite was assessed in a constant volume combustion cell (13 cm^3), from which the pressure history and optical emission during combustion can be obtained simultaneously. Figure 2a shows the schematic of the combustion cell, which is composed of a pressure sensor and an optical detector. Pressurization rates obtained from the pressure history data, which mimic the burning rate, are used to evaluate the reactivity. Burning times were also obtained by measuring the peak width at half-maximum (fwhm) of the optical emission trace.[5,37] Supporting Information Table S1 summarizes the combustion cell results for all the nanothermites in this study.

Figure 2b shows the pressure and optical-emission trace for Al/$Bi(IO_3)_3$ composites. The peak pressure and burning time are ∼4.7 MPa and ∼170 μs, respectively. The burning time is considerably longer than the corresponding pressure rise time, implying that decomposition of iodates occurs prior to the primary reaction of the thermite, suggesting that the thermite burning rate is limited by the aluminum fuel release, rather than oxidizer availability. The temporal pressure of the three metal-iodate-based nanothermites are shown in Figure 2c. All three pressure traces show a rapid rise, of ∼1 μs, achieving a peak pressure of 4−5 MPa with the Cu > Bi > Fe.

For comparison, the reactivity of metal iodates thermite prepared by conventional physical mixing method was also evaluated. The pressurization rate results of metal-iodate-based thermites produced by two approaches were listed in Table 1.

Table 1. Peak Pressure, Pressurization Rate, and Burning Time of Metal-Iodate-Based Nanothermites Made by Electrospraying (ES) and Physical Mixing (PM)[a]

thermite	pressure (MPa)	pressurization (GPa/s)	burning time (μs)
ES Al/$Bi(IO_3)_3$	4.5	3816	235
PM Al/$Bi(IO_3)_3$	0.73	53	298
ES Al/$Cu(IO_3)_2$	4.9	3966	238
PM Al/$Cu(IO_3)_2$	0.14	0.07	2162
ES Al/$Fe(IO_3)_3$	4.0	3186	161
PM Al/$Fe(IO_3)_3$	0.17	0.10	3667

[a]All the composites contain 5% NC (by weight). 25.0 mg sample in each test.

The results show that the pressurization rate of electrosprayed Al/$Bi(IO_3)_3$ composites is approximately 2 orders of magnitude higher than the physical mixed thermites, while the Al/$Cu(IO_3)_2$ and Al/$Fe(IO_3)_3$ systems are more than 4 orders of magnitude higher, relative to the physically mixed thermites. The increase in reactivity of the electrosprayed sample can be attributed to the unique porous inner structure combined with energetic gas generator nitrocellulose which we have previously shown minimizes sintering among nanoparticles.[22]

Similar to what we have observed for Al/CuO composites,[22] the physically mixed $Bi(IO_3)_3$, $Cu(IO_3)_2$, and $Fe(IO_3)_3$ nanothermites have a much longer burning time than that of the corresponding electrosprayed nanothermites, as Figure 2d shows.

The reactivity difference between metal-iodate-based and metal oxide-based thermites was compared. The peak pressure and pressurization rate of the two thermites were simultaneously obtained, as listed in Table 2. The reactivity of the metal-iodate-based thermite is much higher than the reactivity of the corresponding metal-oxide-based thermite even though the size of metal iodate nanoparticles is larger. Specifically, the so-called weak thermite, Al/Fe_2O_3, has a pressure and pressurization rate of only 0.06 MPa and 0.02 GPa/s, respectively. While the corresponding iron-based iodate, Al/$Fe(IO_3)_3$, achieves 1.9 MPa and 590 GPa/s, as shown in Figure 3a. As discussed in our previous work,[38] Al/Fe_2O_3 nanothermite combustion pressure and optical emission signals appear concurrently (Figure 3b), and it has been suggested that oxidizer decomposition is the rate limited step. In contrast, Al/$Fe(IO_3)_3$ features a very rapid pressure increase followed by a prolonged optical emission profile, indicating the burning is rate limited by the aluminum fuel. These results show the advantages of using strong oxidizers, with rapid oxygen release kinetics in nanothermite formulations.

The adiabatic flame temperatures (AFT) of the three metal-iodate- and metal-oxide-based thermites have been calculated and are listed in Table 2. Since there are no experimental data for thermochemical properties of these metal iodates, the theoretical estimate results were adopted.[39] These results are then employed in the Cheetah code, assuming the sample is in the maximum density and the volume of the burning product is constant.[40,41] Generally, the flame temperatures of the three metal-iodate-based thermite reactions are roughly the same, ∼4050 K, which is >1000 K higher than that of the corresponding metal-oxide-based thermites. The high reaction temperature can largely improve the potential biocidal performance for its additional thermal activities which can synergistically function with the released iodine.

To investigate the ignition mechanism, the nanothermite samples were coated on a Pt wire with a diameter of 76 μm and joule heated in air at a heating rate of 5×10^5 K s^{-1}, as schematically shown in Figure 4a. The Al/$Bi(IO_3)_3$ composites reveal a violent reaction, with an ignition temperature of 590 °C. The ignition temperatures of $Cu(IO_3)_2$-based and $Fe(IO_3)_3$-based nanothermites is 560 and 550 °C, respectively,

Table 2. Pressure Cell Results of Physically Mixed Nanothermites[a]

oxidizer	pressure (MPa)	pressurization (GPa/s)	burning time (μs)	AFT (K)	stoichiometric ratio
Bi_2O_3, 90−210 nm	1.0	54	240	2333	1.3
$Bi(IO_3)_3$, ∼90 nm	2.3	770	150	4062	1.0
CuO, ∼50 nm	1.1	100	220	3054	1.0
$Cu(IO_3)_2$, ∼200 nm	1.8	225	170	4061	1.0
Fe_2O_3, ∼50 nm	0.06	0.02	3330	3027	1.0
$Fe(IO_3)_3$, ∼70 nm	1.9	590	170	4043	1.0

[a]Sample mass: 25.0 mg. All the composites contain no NC. The AFT of Al/Bi_2O_3 thermite is only 3031 K. (Because this was a fuel lean mixture, stoichiometric ratio = 1, to optimize pressurization rate.)

DOI: 10.1021/acsami.5b04589
ACS Appl. Mater. Interfaces XXXX, XXX, XXX−XXX

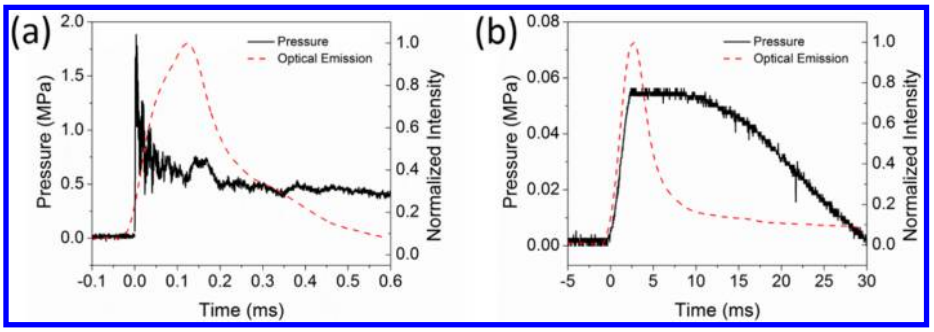

Figure 3. Pressure and optical emission profiles of (a) Al/$Fe(IO_3)_3$ and (b) Al/Fe_2O_3 nanothermite reactions.

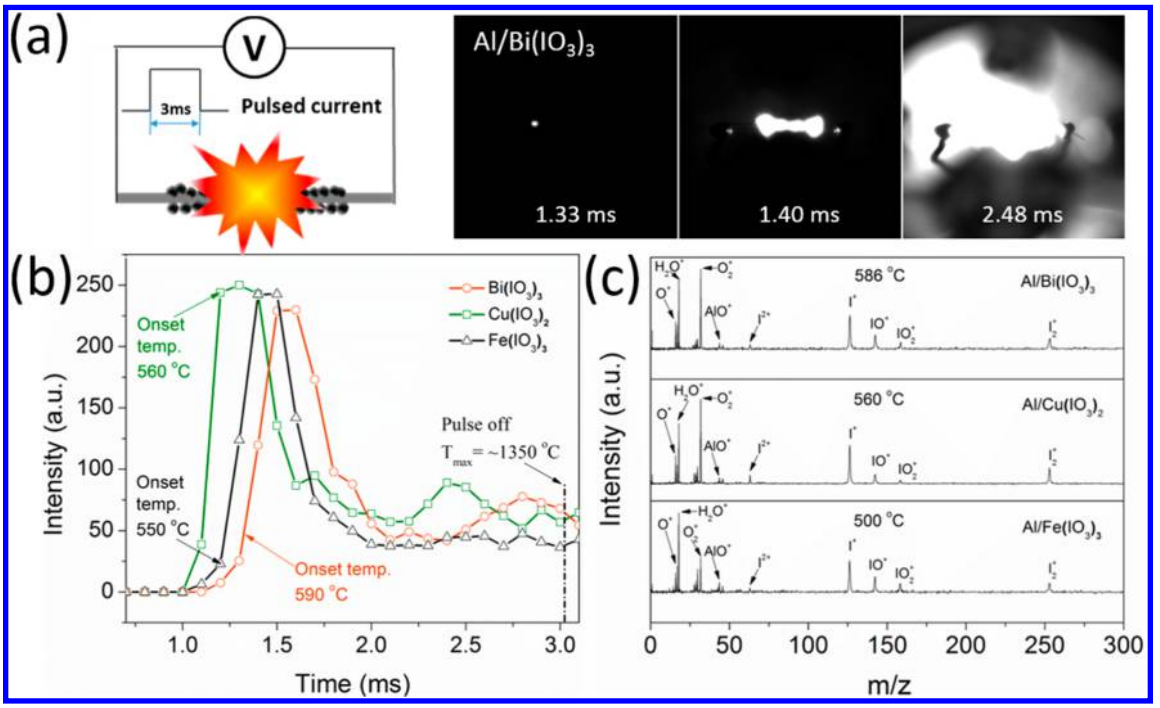

Figure 4. (a) T-Jump wire ignition method, and burning snapshots of Al/$Bi(IO_3)_3$ composites. (b) Temporal profile of oxygen release upon heating the three different metal iodates. (c) T-Jump TOFMS results for the $Bi(IO_3)_3$-based, $Cu(IO_3)_2$-based, and $Fe(IO_3)_3$-based thermite made by electrospray (5% NC, by weight). Note: The heating pulse time was 3.0 ms.

which is much lower than that of corresponding CuO-based (770 °C) and Fe_2O_3-based nanothermites (1140 °C). The low ignition temperature is indicative that the metal iodate salts release oxygen at a relatively low temperature.[5] To further confirm this, the wire within the extraction region of a mass spectrometer, i.e., T-jump/time-of-flight mass spectrum (T-Jump/TOFMS), was employed to investigate the oxygen release properties of the three metal iodates.[37]

Reactivity of a thermite can be evaluated by the explosion characterization parameters such as peak pressure, pressurization rate, and burn time in a confined container (Figure 2a). Especially, the pressurization rate is directly proportional to the burn rate of the thermite. In the previous work, it is found that the reactivity is closely related to its oxygen release behavior at high heating rates.[42] Figure 4b shows the temporal profile for oxygen from metal iodates in T-Jump/TOFMS, from which the oxygen release temperature can be obtained, and the oxygen release behavior of different oxidizers at high heating rates can be compared. It is found that the onset temperature of oxygen release for $Bi(IO_3)_3$, $Cu(IO_3)_2$, and $Fe(IO_3)_3$ nanoparticles is 490, 450, and 475 °C, respectively, and thus insensitive to structure. Interestingly, it is worth noting that while $Bi(IO_3)_3$ releases oxygen at 490 °C, and Bi_2O_3 releases gas phase oxygen at ~1350 °C, they both show a similar ignition temperature of ~590 °C.[43] The results imply that $Bi(IO_3)_3$ and Bi_2O_3 have different initiation mechanisms. For $Bi(IO_3)_3$, it is obvious that oxygen release from oxidizer contributes to the ignition of nanothermite, while its condensed phase appears to be the initiation mechanism for the Al/Bi_2O_3 nanothermite.

As Figure 4b shows, all of the oxygen release traces show a rapid rise. The oxygen release from $Cu(IO_3)_2$ initiates at 450 °C, and reaches it maximum in 0.20 ms, significantly outperforming the commercial CuO nanoparticles, whose rise time is 1.0 ms,[33] revealing its fast oxygen release kinetics at high heating rates. Oxygen release profiles of $Fe(IO_3)_3$ and $Bi(IO_3)_3$ nanoparticles are very similar to that of $Cu(IO_3)_3$, implying, not surprisingly, that all metal iodate nanoparticles release oxygen in a similar manner. It is worth noting that the decomposition of iodates occurs prior to the thermite ignition, suggesting that gas phase oxygen release is critical to ignition.

The metal-iodate-based nanothermites were also rapidly heated in the T-Jump/TOFMS to determine temporal

DOI: 10.1021/acsami.5b04589
ACS Appl. Mater. Interfaces XXXX, XXX, XXX−XXX

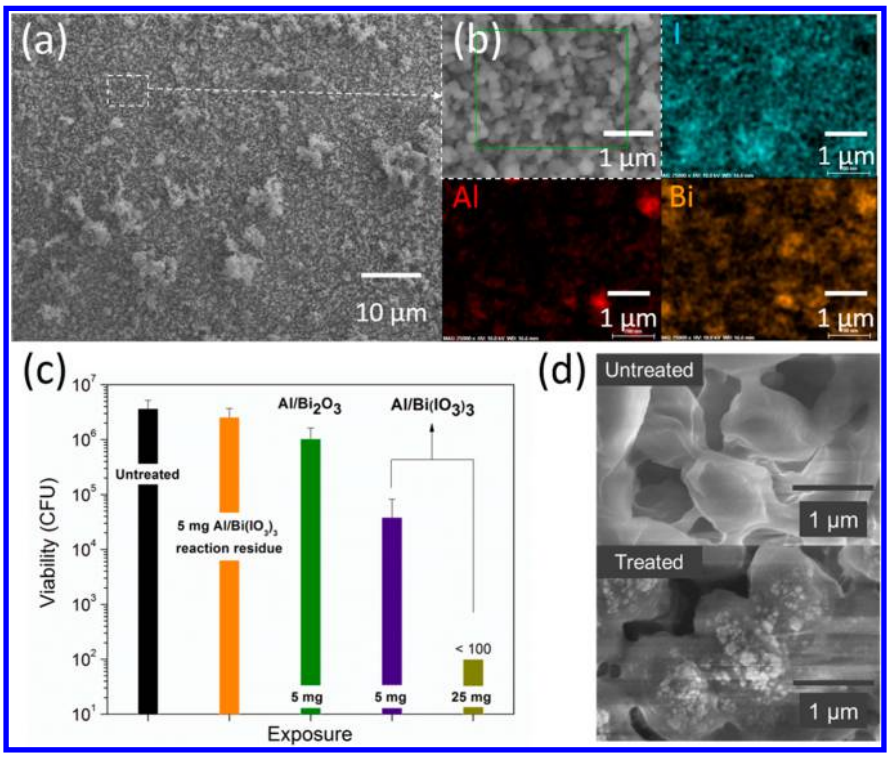

Figure 5. (a, b) SEM and energy dispersive X-ray spectroscopy (EDS) results of $Al/Bi(IO_3)_3$ thermite reaction products. (c) CFU counts from the spores treated by 5.0 mg $Al/Bi(IO_3)_3$ postcombustion products, 5.0 mg Al/Bi_2O_3 thermite reaction, and 5.0 mg and 25.0 mg $Al/Bi(IO_3)_3$ thermite reactions. (d) SEM images of spores before (top) and after (bottom) undergoing the $Al/Bi(IO_3)_3$ thermite reaction (5.0 mg). Note: all the composites are produced by electrospraying with 5% NC (by weight). The labeled numbers in part c are survival ratios of spores.

speciation. As shown in Figure 4c, iodine and oxygen species are detected in all three metal-iodate-based thermites reactions. The intensities of oxygen and iodine species, in all of the samples, reach their maximum values between 500 and 600 °C, revealing the major weight loss event happening during that period, and is consistent with TGA results (Supporting Information).

3.3. Sporicidal Performance. The ability of metal-iodate-based thermites to produce high heat, pressure, and iodine makes them ideal biocidal energetic materials with potential synergistic killing mechanisms. To test the sporicidal performance of metal iodate-based thermites, a spore inactivation experiment was conducted in the combustion cell (V = 13 cm^3, see Figure 2a). Aluminum foil coupons deposited with or without ~7×10^6 CFU *Bacillus thuringiensis* spores were placed within the combustion chamber around the wire coil that ignites the thermite reaction. The control experiment of $Al/Bi(IO_3)_3$ thermite reaction without spores shows that iodine was released after reaction and uniformly dispersed within the layer of postcombustion products (Figure 5a,b). By loading different quantities of $Al/Bi(IO_3)_3$ thermite in the combustion cell, the survival ratios of *Bacillus thurigiensis* spores on coupons were measured after the thermite reactions (Figure 5c). Spores exposed to 5.0 mg and 25.0 mg of thermite reaction products had a 2 log or a >4 log reduction in their viability (i.e., the ability to form bacterial colonies), respectively. Alternatively, similar tests by employing the reaction of 5.0 mg Al/Bi_2O_3 thermites show that the viability of spores decreased by 28%. The major difference of these two thermite systems is that iodate-based composites can generate free iodine through a thermite reaction, which has been widely confirmed as a biocidal agent. Therefore, except for the pressure and thermal stresses which were also generated from the combustion of Al/Bi_2O_3 thermites, the combustion of $Al/Bi(IO_3)_3$ thermites exposes spores to the additional biocidal stress of iodine. We estimated that the released iodine efficiently contributed to 27% loss of spore viability (28% − 1%), while the other effects from pressure, heat, and other reaction products such as Al_2O_3 and Bi contributed to the majority of the loss as confirmed by the result after the Al/Bi_2O_3 reaction (Figure 5c). Figure 5c shows that the postreaction products of Al_2O_3 and Bi induced viability reduction of spores by 30%, implying that the other heat and pressure stresses contributed to a 42% loss of spore viability (72% − 30%). Given that other reactions of metal iodate thermites ($Al/Bi(IO_3)_3$ and $Al/Cu(IO_3)_2$) also led to uniform iodine release (Supporting Information Figures S13 and S14) and demonstrate higher sporicidal capabilities compared with the corresponding oxide-based thermite reactions (Supporting Information Figure S15), it is proposed that the metal iodate thermite system can be recognized as an effective biocidal agent.

The SEM images of spores (Figure 5d) further demonstrate that fine particles were deposited on the spore surfaces after the 5.0 mg $Al/Bi(IO_3)_3$ thermite reaction. There is some precedent for cell death in the absence of morphological damage.[43] However, interestingly, there is no gross morphological change in the spores after the thermite reaction, suggesting that the thermite reaction has not compromised the spore structure, although the viability has been reduced by 2 orders of magnitude (Figure 5c). Previously, we have shown that, during rapid heating, spores maintained most of their viability until the spore coat was melted.[44] Herein, it is further found that, by applying iodine, the spores were killed before changing morphologies, indicating the superiority in efficacy of the

DOI: 10.1021/acsami.5b04589
ACS Appl. Mater. Interfaces XXXX, XXX, XXX−XXX

$Bi(IO_3)_3$-based thermite complex in killing spores compared with simple rapid heating.

4. CONCLUSION

This work reports the formation of metal-iodate-based thermites which have superior performance as sporicidal agents. Three different metal iodate nanoparticles were synthesized and incorporated into energetic composites with nanoaluminum by electrospray or physical mixing, forming highly reactive nanothermites. We characterized the reactivity using combustion cell and fast-heating wire experiments. The pressure and pressurization rate of metal-iodate-based thermites are several times higher than the corresponding oxide-based thermites, and the reactivity could be further promoted by using the electrospray technique to assemble the metal-iodate-based thermites. The thermal decomposition properties of metal iodates, as well as the reaction mechanisms of the related thermites, were separately investigated by TGA/DSC, and TOF-MS. The results show that the metal iodates decompose into their corresponding metal oxide, oxygen, and iodine before the aluminothermic reaction takes place. The sporicidal performance of the metal-iodate-based thermites was also assessed, and the results showed that they outperform the corresponding metal-oxide-based thermites. The working mechanism was proposed as a synergistic effect of heat/pressure and iodine production from the highly reactive metal-iodate-based thermite reaction. This combination has a much higher sporicidal rate than the individual effect of either heat/pressure (from the metal-oxide-based thermite reaction) or iodine (from the burning residue of metal-iodate-based thermite reaction).

■ ASSOCIATED CONTENT

Supporting Information

Characterization of the three different metal iodates nanoparticles was shown, including SEM and TEM images, as well as thermal decomposition results. The SEM images of electrosprayed metal-oxide-based thermites and physically mixed metal-iodate-based thermites. The combustion cell results of all three kinds of metal-iodate-based thermites and corresponding metal-oxide-based thermites. The burning snapshots of $Al/Cu(IO_3)_2$ and $Al/Fe(IO_3)_3$ composites on the wire. The SEM images and EDS results of the postcombustion products from $Al/Cu(IO_3)_2$ and $Al/Fe(IO_3)_3$ composite thermite reaction. The Supporting Information is available free of charge on the ACS Publications website at DOI: 10.1021/acsami.5b04589.

■ AUTHOR INFORMATION

Corresponding Author

*Phone: 301-405-4311. E-mail: mrz@umd.edu.

Present Address

§Department of Safety Engineering, Nanjing University of Science and Technology, Nanjing, Jiangsu 210094, China.

Author Contributions

The manuscript was written through contributions of all authors. All authors have given approval to the final version of the manuscript.

Notes

The authors declare no competing financial interest.

■ ACKNOWLEDGMENTS

This work was supported by the Defense Threat Reduction Agency and the Army Research Office. We acknowledge the support of the Maryland Nanocenter and its NispLab. The NispLab is supported in part by the NSF as a MRSEC Shared Experimental Facility. H.-Y.W. is grateful for the financial support from China Scholarship Council.

■ REFERENCES

(1) Rossi, C.; Estéve, A.; Vashishta, P. Nanoscale Energetic Materials. *J. Phys. Chem. Solids* **2010**, *71*, 57−58.
(2) Weismiller, M. R.; Malchi, J. Y.; Lee, J. G.; Yetter, R. A.; Foley, T. J. Effects of Fuel and Oxidizer Particle Dimensions on the Propagation of Aluminum Containing Thermites. *Proc. Combust. Inst.* **2011**, *33*, 1989−1996.
(3) Moore, K.; Pantoya, M. L.; Son, S. F. Combustion Behaviors Resulting from Bimodal Aluminum Size Distributions in Thermites. *J. Propul. Power* **2007**, *23*, 181−185.
(4) Pantoya, M. L.; Granier, J. J. Combustion Behavior of Highly Energetic Thermites: Nano versus Micron Composites. *Propellants, Explos., Pyrotech.* **2005**, *30*, 53−62.
(5) Jian, G. Q.; Feng, J. Y.; Jacob, R. J.; Egan, G. C.; Zachariah, M. R. Super-reactive Nanoenergetic Gas Generators Based on Periodate Salts. *Angew. Chem., Int. Ed.* **2013**, *52*, 9743−9746.
(6) Granier, J. J.; Pantoya, M. L. Laser Ignition of Nanocomposite Thermites. *Combust. Flame* **2004**, *138*, 373−383.
(7) Blobaum, K. J.; Reiss, M. E.; Plitzko, J. M.; Weihs, T. P. Deposition and Characterization of a Self-propagating CuO_x/Al Thermite Reaction in a Multilayer Foil Geometry. *J. Appl. Phys.* **2003**, *94*, 2915−2922.
(8) Schoenitz, M.; Ward, T. S.; Dreizin, E. L. Fully dense Nano-Composite Energetic Powders Prepared by Arrested Reactive Milling. *Proc. Combust. Inst.* **2005**, *30*, 2071−2078.
(9) Blobaum, K. J.; Wagner, A. J.; Plitzko, J. M.; Van Heerden, D.; Fairbrother, D. H.; Weihs, T. P. Investigating the Reaction Path and Growth Kinetics in CuOx/Al Multilayer Foils. *J. Appl. Phys.* **2003**, *94*, 2923−2929.
(10) Petrantoni, M.; Rossi, C.; Salvagnac, L.; Conédéra, V.; Estève, A.; Tenailleau, C.; Alphonse, P.; Chabal, Y. J. Multilayered Al/CuO Thermite Formation by Reactive Magnetron Sputtering: Nano versus Micro. *J. Appl. Phys.* **2010**, *108*, 084323.
(11) Zhang, K.; Rossi, C.; Ardila Rodriguez, G. A. Development of a Nano-Al/CuO Based Energetic Material on Silicon Substrate. *Appl. Phys. Lett.* **2007**, *91*, 113117.
(12) Umbrajkar, S. M.; Seshadri, S.; Schoenitz, M.; Hoffmann, V. K.; Dreizin, E. L. Aluminum-Rich Al-MoO_3 Nanocomposite Powders Prepared by Arrested Reactive Milling. *J. Propul. Power* **2008**, *24*, 192−198.
(13) Ward, T. S.; Chen, W.; Schoenitz, M.; Dave, R. N.; Dreizin, E. L. A Study of Mechanical Alloying Processes Using Reactive Milling and Discrete Element Modeling. *Acta Mater.* **2005**, *53*, 2909−2918.
(14) Kim, S. H.; Zachariah, M. R. Enhancing the Rate of Energy Release from Nanoenergetic Materials by Electrostatically Enhanced Assembly. *Adv. Mater.* **2004**, *16*, 1821−1825.
(15) Tillotson, T. M.; Gash, A. E.; Simpson, R. L.; Hrubesh, L. W.; Satcher, J. H., Jr.; Poco, J. F. Nanostructured Energetic Materials Using Sol−Gel Methodologies. *J. Non-Cryst. Solids* **2001**, *285*, 338−345.
(16) Seo, H. S.; Kim, J. K.; Kim, J. W.; Kim, H. S.; Koo, K. K. Thermal Behavior of Al/MoO_3 Xerogel Nanocomposites. *J. Ind. Eng. Chem.* **2014**, *20*, 189−193.
(17) Rossi, C.; Zhang, K.; Esteve, D.; Alphonse, P.; Tailhades, P.; Vahlas, C. Nanoenergetic Materials for MEMS: a Review. *J. Microelectromech. Syst.* **2007**, *16*, 919−931.
(18) Subramanium, S.; Hasan, S.; Bhattacharya, S.; Gao, Y.; Apperson, S.; Hossain, M.; Shede, R. V.; Gangopadhyay, S.; Render, R.; Kapper, P.; Nicolich, S. Self-assembled Ordered Energetic Composites of CuO Nanorods and Nanowells and Al Nanoparticles with High Burn Rates. *Mater. Res. Soc. Symp. Proc.* **2005**, *896*, 9.

DOI: 10.1021/acsami.5b04589
ACS Appl. Mater. Interfaces XXXX, XXX, XXX−XXX

(19) Shende, R.; Subramanian, S.; Hasan, S.; Apperson, S.; Thiruvengadathan, R.; Gangopadhyay, K.; Gangopadhyay, S.; Redner, P.; Kapoor, D.; Nicolich, S.; Balas, W. Nanoenergetic Composites of CuO Nanorods, Nanowires, and Al-Nanoparticles. *Propellants, Explos., Pyrotech.* **2008**, *33*, 122−130.
(20) Malchi, J. Y.; Foley, T. J.; Yetter, R. A. Electrostatically Self-assembled Nanocomposite Reactive Microspheres. *ACS Appl. Mater. Interfaces* **2009**, *1*, 2420−2423.
(21) Séverac, F.; Alphonse, P.; Estève, A.; Bancaud, A.; Rossi, C. High-Energy Al/CuO Nanocomposites Obtained by DNA-Directed Assembly. *Adv. Funct. Mater.* **2012**, *22*, 323−329.
(22) Wang, H. Y.; Jian, G. Q.; Egan, G. C.; Zachariah, M. R. Assembly and Reactive Properties of Al/CuO Based Nanothermite Microparticles. *Combust. Flame* **2014**, *161*, 2203−2208.
(23) Nicholson, W. L.; Munakata, N.; Horneck, G.; Melosh, H. J.; Setlow, P. Resistance of Bacillus Endospores to Extreme Terrestrial and Extraterrestrial Environments. *Microbiol. Mol. Biol. Rev.* **2000**, *64*, 548−572.
(24) Setlow, P. Spores of Bacillus Subtilis: their Resistance to and Killing by Radiation, Heat and Chemicals. *J. Appl. Microbiol.* **2006**, *101*, 514−525.
(25) Leggett, M. J.; McDonnell, G.; Denyer, S. P.; Setlow, P.; Maillard, J. Y. Bacterial Spore Structures and their Protective Role in Biocide Resistance. *J. Appl. Microbiol.* **2012**, *113*, 485−498.
(26) Johnson, C. E.; Higa, K. T. Presented at *MRS Meeting Iodine-Rich Biocidal Reactive Materials*, Boston, 25−30 (11, 2012).
(27) Mulamba, O.; Hunt, E. M.; Pantoya, M. L. Neutralizing Bacterial Spores Using Halogenated Energetic Reactions. *Biotechnol. Bioprocess Eng.* **2013**, *18*, 918−925.
(28) He, C.; Zhang, J.; Shreeve, J. M. Dense Iodine-Rich Compounds with Low Detonation Pressures as Biocidal Agents. *Chem. - Eur. J.* **2013**, *19*, 7503−7509.
(29) Fischer, D.; Klapotke, T.; Stierstorfer, J. R. Synthesis and Characterization of Guanidinium Difluoroiodate, $[C(NH2)-3]^{+}[IF2O2]^{-}$ and its Evaluation as an Ingredient in Agent Defeat Weapons. *Z. Anorg. Allg. Chem.* **2011**, *637*, 660−665.
(30) Aly, Y.; Zhang, S.; Schoenitz, M.; Hoffmann, V. K.; Dreizin, E. L.; Yermakov, M.; Indugula, R.; Grinshpun, S. A. Iodine-containing Aluminum-based Fuels for Inactivation of Bioaerosols. *Combust. Flame* **2014**, *161*, 303−310.
(31) Feng, J. Y.; Jian, G. Q.; Liu, Q.; Zachariah, M. R. Passivated Iodine Pentoxide Oxidizer for Potential Biocidal Nanoenergetic Applications. *ACS Appl. Mater. Interfaces* **2013**, *5*, 8875−8880.
(32) Sullivan, K. T.; Piekiel, N. W.; Chowdhury, S.; Wu, C.; Zachariah, M. R.; Johnson, C. E. Ignition and Combustion Characteristics of Nanoscale Al/$AgIO_3$: A Potential Energetic Biocidal System. *Combust. Sci. Technol.* **2010**, *183*, 285−302.
(33) Jian, G. Q.; Chowdhury, S.; Sullivan, K.; Zachariah, M. R. Nanothermite Reactions: Is Gas Phase Oxygen Generation from the Oxygen Carrier an Essential Prerequisite to Ignition? *Combust. Flame* **2013**, *160*, 432−437.
(34) Jian, G. Q.; Piekiel, N. W.; Zachariah, M. R. Time-resolved Mass Spectrometry of Nano-Al and Nano-Al/CuO Thermite under Rapid Heating: a Mechanistic Study. *J. Phys. Chem. C* **2012**, *116*, 26881−26887.
(35) Zhou, L.; Piekiel, N.; Chowdhury, S.; Zachariah, M. R. T-Jump/time-of-flight Mass Spectrometry for Time-Resolved Analysis of Energetic Materials. *Rapid Commun. Mass Spectrom.* **2009**, *23*, 194−202.
(36) Wang, H. Y.; Jian, G. Q.; Yan, S.; DeLisio, J. B.; Huang, C.; Zachariah, M. R. Electrospray Formation of Gelled Nano-Aluminum Microspheres with Superior Reactivity. *ACS Appl. Mater. Interfaces* **2013**, *5*, 6797−6801.
(37) Sullivan, K. T.; Piekiel, N. W.; Wu, C.; Chowdhury, S.; Kelly, S. T.; Hufnagel, T. C.; Fezzaa, K.; Zachariah, M. R. Reactive Sintering: an Important Component in the Combustion of Nanocomposite Thermites. *Combust. Flame* **2012**, *159*, 2−15.
(38) Sullivan, K.; Zachariah, M. R. Simultaneous Pressure and Optical Measurements of Nanoaluminum Thermites: Investigating the Reaction Mechanism. *J. Propul. Power* **2010**, *26*, 467−472.
(39) Jain, A.; Ong, S. P.; Hautier, G.; Chen, W.; Richards, W. D.; Dacek, S.; Cholia, S.; Gunter, D.; Skinner, D.; Ceder, G.; Persson, K. A. The Materials Project: A materials genome approach to accelerating materials innovation. *APL Mater.* **2013**, *1*, 011002.
(40) Howard, W. M.; Souers, P. C.; Vitello, P. A. *Cheetah 6.0 User Manual*; LLNL-SM-416166; Lawrence Livermore National Laboratory: Livermore, CA, 2010.
(41) Hobbs, M. L.; Baer, M. R.; McGee, B. C. JCZS: An Intermolecular Potential Database for Performing Accurate Detonation and Expansion Calculations. *Propellants, Explos., Pyrotech.* **1999**, *24*, 269−279.
(42) Zhou, L.; Piekiel, N. W.; Chowdhury, S.; Zachariah, M. R. Time-resolved Mass Spectrometry of the Exothermic Reaction between Nanoaluminum and Metal Oxides: the Role of Oxygen Release. *J. Phys. Chem. C* **2010**, *114*, 14269−14275.
(43) Davis, C. Enumeration of Probiotic Strains: Review of Culture Dependent and Alternative Techniques to Quantify Viable Bacteria. *J. Microbiol. Methods* **2014**, *103*, 9−17.
(44) Zhou, W. B.; Wu, M. O.; Watt, S. K.; Jian, G. Q.; Lee, V. T.; Zachariah, M. R. Inactivation of Bacterial Spores Subjected to Sub-second Thermal Stress. *Chem. Eng. J.* **2014**, *279*, 578−588.

DOI: 10.1021/acsami.5b04589
ACS Appl. Mater. Interfaces XXXX, XXX, XXX−XXX